

Article

A Voltammetric Sensor for the Determination of Hydroxylamine Using a Polypyrrole Nanotubes-Modified Electrode

Peyman Mohammadzadeh Jahani¹, Hadi Beitollahi^{2,*} and Antonio Di Bartolomeo^{3,*} 

¹ School of Medicine, Bam University of Medical Sciences, Bam 7661771967, Iran; peymanjahani1234@gmail.com

² Environment Department, Institute of Science and High Technology and Environmental Sciences, Graduate University of Advanced Technology, Kerman 7631885356, Iran

³ Dipartimento di Fisica "E.R. Caianiello", Università di Salerno, 84084 Fisciano, Italy

* Correspondence: h.beitollahi@kgut.ac.ir (H.B.); adibartolomeo@unisa.it (A.D.B.)

Abstract: In this work, we develop an electrochemical sensor using a polypyrrole nanotubes-modified graphite screen-printed electrode (PPy NTs/GSPE) for sensing hydroxylamine. The PPy NTs/GSPE-supported sensor has an appreciable electrocatalytic performance and great stability for hydroxylamine oxidation. Compared to a bare graphite screen-printed electrode, we demonstrate that using the PPy NTs/GSPE leads to a significant reduction in the oxidation potential of hydroxylamine. The standard curve shows a linear relationship ranging from 0.005 to 290.0 μM ($R^2 = 0.9998$), with a high sensitivity (0.1349 $\mu\text{A}/\mu\text{M}$) and a narrow limit of detection (LOD) of 0.001 μM . In addition, the PPy NTs/GSPE has satisfactory outcomes for hydroxylamine detection in real specimens.

Keywords: hydroxylamine; polypyrrole nanotubes; electrochemical sensor; voltammetry



Citation: Mohammadzadeh Jahani, P.; Beitollahi, H.; Di Bartolomeo, A. A Voltammetric Sensor for the Determination of Hydroxylamine Using a Polypyrrole Nanotubes-Modified Electrode. *Appl. Sci.* **2022**, *12*, 7485. <https://doi.org/10.3390/app12157485>

Academic Editor: Fethi Bedioui

Received: 16 May 2022

Accepted: 22 July 2022

Published: 26 July 2022

Publisher's Note: MDPI stays neutral with regard to jurisdictional claims in published maps and institutional affiliations.



Copyright: © 2022 by the authors. Licensee MDPI, Basel, Switzerland. This article is an open access article distributed under the terms and conditions of the Creative Commons Attribution (CC BY) license (<https://creativecommons.org/licenses/by/4.0/>).

1. Introduction

Hydroxylamine, NH_2OH , is derived from ammonium as an intermediate during the two primary microbial nitrogen processes of anaerobic ammonium oxidation and nitrification. Hydroxylamine has a variety of industrial and pharmaceutical applications as a raw material [1,2]. The characteristics of hydroxylamine were recently detected following two major events; one involved the deaths of five people in the United States (February 1999), and the other involved the deaths of four people in Japan (June 2000). Moreover, hydroxylamine is a mutagenic, toxic, and harmful agent for living organisms that produces reversible and irreversible physiological alterations [3–5]. Accordingly, from environmental, health, and industrial viewpoints, the achievement of a sensitive analytical method for the detection of trace amounts of hydroxylamine is of remarkable importance.

Various techniques for the detection of hydroxylamine content have been developed, such as spectrophotometric methods [6], high performance liquid chromatography [7], gas chromatography [8], and polarography [9]. In spite of their many advantages, all these methods present some challenges, such as their complexity, expensiveness, the need for advanced equipment, and prolonged execution times [10].

For these reasons, electrochemical techniques are promising candidates for the construction of cost-effective and portable electrochemical sensing systems because of their high stability, lengthy linearity, possibility of miniaturization, simple instrumentation, quick response, and higher sensitivity and selectivity [11–20].

Disposable electrochemical graphite screen-printed electrodes (GSPEs) possess special features, such as low background current, capacity for mass production, cost-effectiveness, and disposability that can compensate for the numerous shortcomings of glassy carbon electrodes and carbon paste electrodes, including difficult cleaning procedures and memory impacts [21–25].

Most bare electrodes used for the electrochemical determination of analyte have multiple restrictions (e.g., low selectivity, high overpotential, and negligible stability in a broad spectrum of solution compositions). Hence, electrode modification can bypass these barriers [26–30]. The mass transfer kinetics can be improved by chemically modified electrodes (CMEs) at low overpotential, which reduces the impacts of interferants and inhibits surface fouling [31–36].

In recent years, nanomaterials have been investigated extensively in various fields, owing to their small size, impressive porosity, large specific surface area, and special physicochemical traits [37–41]. Several advances in the field of nanomaterials have been made to improve the performance of the sensors [42–45].

Conducting polymer nanomaterials have many applications in the fields of optoelectronics, electronics, (bio)sensing systems, and energy storage [46]. Polypyrrole (PPy) nanomaterials are popular polymers because of their admirable electronic conductivity, high stability, ease of construction, and appreciable biocompatibility. In addition, their outstanding electrical properties are related to the resonance of the delocalized π electrons present in the entire carbon chain of the polymer structure [47,48].

It should be noted that conductive polymers such as the PPy nanomaterials can be employed in various types of electrochemical equipment, such as voltammetric and corrosion sensors, because of their great electrical and electrochemical windows. In addition, the morphology of polypyrrole nanomaterials affects the catalytic properties. In particular, the PPy NTs are of unparalleled utility for sensing systems owing to their appreciable electron transduction, large surface areas, huge surface functionalities and porous structure [49–51].

In this paper, a graphite screen-printed electrode modified with polypyrrole nanotubes was fabricated for the determination of hydroxylamine. Such an electrode has not been tested for this purpose before. The fabricated sensor exhibited an enhanced catalytic performance for hydroxylamine oxidation.

2. Experimental Procedure

2.1. Instrumentation

A Tescan Field Emission Scanning Electron Microscope (FE-SEM, Mira3-Xum, Brno, Czech Republic) was used to capture FE-SEM images of the polypyrrole nanotubes. A PAN analytical instrument (x, pert3, Almelo, The Netherlands) was applied to obtain the X-ray diffraction (XRD) pattern of the polypyrrole nanotubes. Moreover, Fourier transform infrared spectroscopy (FT-IR) was carried out on a Bruker spectrometer with KBr pellets (Tensor-2, Bruker Corporation, Hanau, Germany) and was applied to obtain the functional groups of the polypyrrole nanotubes. An Autolab electrochemical instrument (Metrohm-PGSTAT302N, Metrohm Autolab B.V., 3526 KM, Utrecht, The Netherlands) was used for the voltammetric measurements. The experimental settings were explored using General Purpose Electrochemical System (GPES) software. The three-component DropSens screen-printed electrode (DRP-110, DropSens, Oviedo, Spain) consisted of a graphite working electrode, a silver pseudo-reference electrode, and a graphite counter electrode. All pH adjustments were performed using a Metrohm 710 pH meter (Metrohm Autolab B.V., 3526 KM, Utrecht, The Netherlands).

2.2. Materials

All chemicals and reagents were in a state of analytical purity, with no need for further purification. Hydroxylamine, methyl orange, iron (III) chloride (FeCl_3), pyrrole, and ethanol were obtained from Sigma-Aldrich (St. Louis, MO, USA).

The preparation of a 0.1 M phosphate buffer solution (PBS) was carried out using orthophosphoric acid and the respective salts in a pH range between 2 and 9.

2.3. Synthesis of the PPy NTs

The preparation of the PPy NTs was performed through pyrrole monomer oxidation with iron (III) chloride in exposure to methyl orange as a structure-guiding agent [52].

Thus, FeCl_3 (3.888 g; 23 mmol) with methyl orange (0.784 g; 2.3 mmol) were dissolved in deionized water (480 mL) followed by the addition of pyrrole (0.84 mL; 12.1 mmol), and the solution was stirred at an ambient temperature for 24 h. Then, the deionized water/ethanol (with proportions of 70:30) was used to thoroughly wash the attained PPy NTs precipitate until the filtrate was colorless and neutral, followed by vacuum-drying at 65 °C for 20 h.

2.4. Modified Electrode Fabrication

The modification of the GSPEs with the PPy NTs was performed using the drop-casting method. Briefly, 1 mg of the synthesized PPy NTs was poured into 1 mL of pure water under ultra-sonication for one hour. Then, 4 μL of the PPy NTs suspension was placed onto the working electrode surface of the GSPE. After solvent evaporation at an ambient temperature, the electrode was stored for future use.

2.5. Real Sample

The real river and well water specimens were filtered (with a 0.45 μm filter) prior to analysis using the standard addition method, and the variable hydroxylamine contents were spiked in the specimens.

3. Results and Discussion

3.1. Characterization of the PPy NTs

The FE-SEM image captured of the PPy NTs is shown in Figure 1, illustrating a one-dimensional nanotube structure of the PPy that is 87–150 nm in diameter and several micrometers in length, which is consistent with that reported in the previous literature [53].

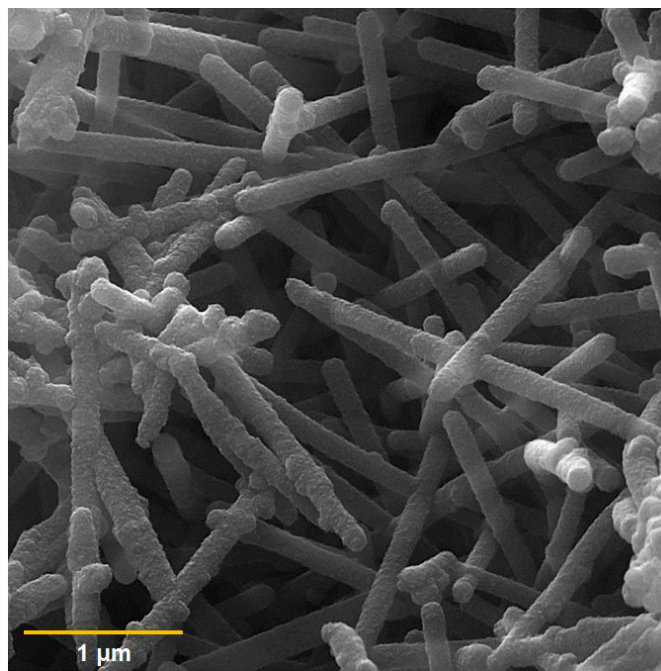


Figure 1. FE-SEM image of the PPy NTs.

The FT-IR spectrum of the PPy NTs ranged from 400 to 4000 cm^{-1} (Figure 2). The peaks at 1552 and 1450 cm^{-1} can be related to symmetric and asymmetric polypyrrole ring stretching bonds, sequentially. Moreover, the peak at 1038, 1333, 1110, and 1603 cm^{-1} corresponds to C-H deformation vibrations, C-N stretching vibrations, C-C stretching, and C=C stretching, sequentially. A broad peak at 3446 cm^{-1} can also be related to the N-H stretching vibrations of the pyrrole ring. The successful PPy polymer formation is evident based on the FT-IR patterns [52,54].

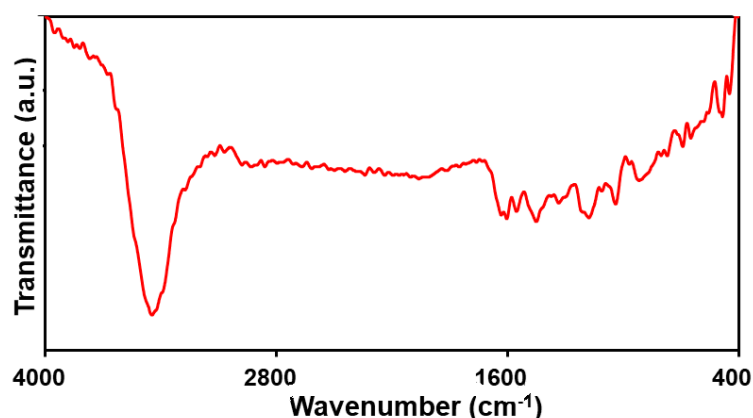


Figure 2. The FT-IR spectrum obtained of the PPY NTs.

The XRD pattern obtained of the PPY NTs can be seen in Figure 3. There is a wide peak at the 2θ value of 24.8° (Figure 3). The wide peak indicates the amorphous polymer and intramolecular stacking structure [55].

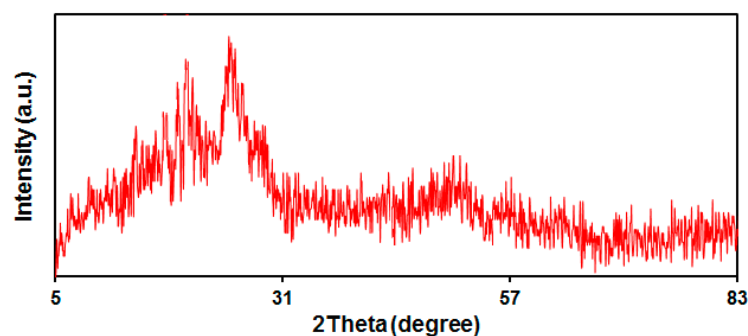


Figure 3. XRD pattern of the PPY NTs.

3.2. Electrochemical Behavior of Hydroxylamine on the PPY NTs/GSPE

Since the selected analyte oxidation depends on the pH, the influence of the pH on the hydroxylamine oxidation was determined for the optimization of the operational conditions to reach the highest response. The electrochemical behavior of hydroxylamine on the PPY NTs/GSPE was examined in 0.1 M PBS at variable pHs of 2.0–9.0 using cyclic voltammetry (CV) (Figure 4). Reportedly, the hydroxylamine electro-oxidation on the PPY NTs/GSPE surface was higher in neutral conditions than in an alkaline medium or acidic medium (Figure 4A). Consequently, a pH of 7.0 was chosen as optimal for the hydroxylamine electro-oxidation on the PPY NTs/GSPE surface. In addition, it was discovered that the values of the peak potential shift to lower values with increasing pH, as shown in Figure 4B. Thus, the peak potential is linearly dependent on the pH, according to the following equation: $E_p \text{ (mV)} = -59.786 \text{ pH} + 1208.6$ ($R^2 = 0.9997$). The value of the slope (-59.786 mV/pH) was very close to the theoretical value (-59 mV/pH), indicating that the same electron and proton numbers participate in the electrochemical oxidation process.

The electrochemical behavior of $100.0 \mu\text{M}$ hydroxylamine in the buffer solution (pH 7.0) was illustrated by using differential pulse voltammetry (DPV) techniques on the surfaces of bare GSPE (Figure 5, curve b) and the PPY NTs/GSPE (Figure 5, curve a). The anodic peak potential was approximately 1000 mV for the hydroxylamine oxidation on the bare GSPE, while it was approximately 790 mV on the PPY NTs/GSPE. On other hand, the GSPE exhibited a minimal current ($4.0 \mu\text{A}$), and the PPY NTs/GSPE exhibited an elevation in the oxidation current ($14.5 \mu\text{A}$). Accordingly, the greatest electrocatalytic impact on hydroxylamine oxidation was on the surface of the PPY NTs/GSPE as opposed to the bare GSPE, which was caused by increasing the simplification of the electron transfer process.

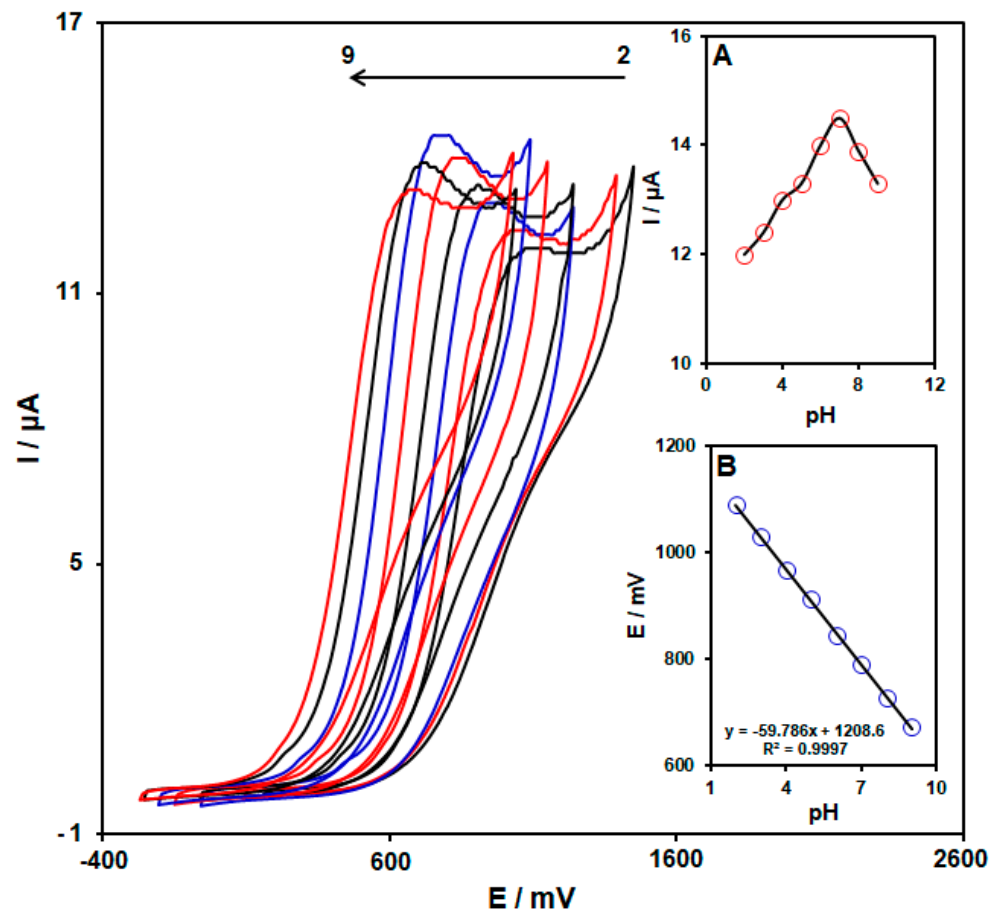


Figure 4. CV response of 100.0 μM hydroxylamine on the PPy NTs/GSPE in 0.1 M PBS at different pH values (2.0–9.0). (A) Plot of the oxidation peak current of hydroxylamine as a function of the pH solution. (B) Plot of the oxidation peak potential of hydroxylamine as a function of the pH solution.

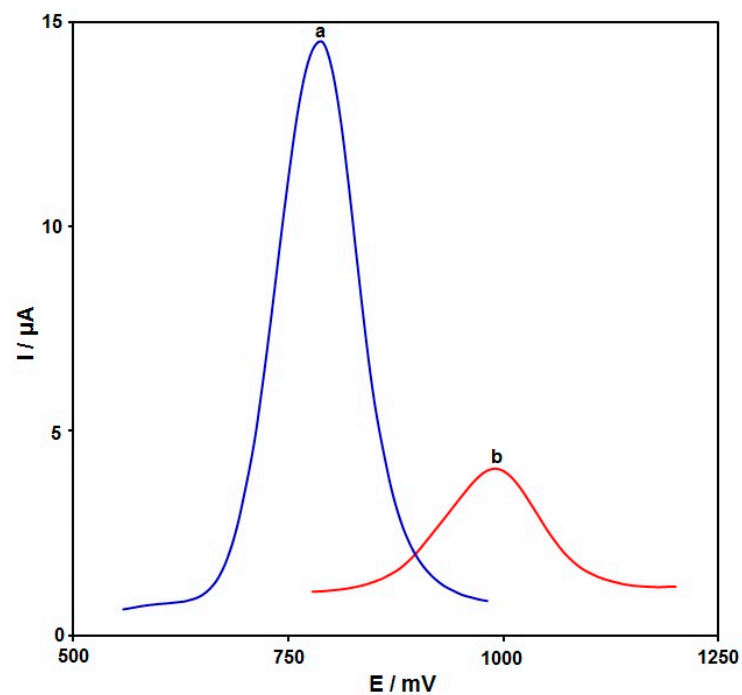


Figure 5. DPV recorded for (a) the PPy NTs/GSPE and (b) the un-modified GSPE in 0.1 M PBS at pH = 7 with 100.0 μM hydroxylamine at a 50-mV/s scan rate.

3.3. Scan Rate Exploration

The influence of the scan rate (v) on the hydroxylamine (100.0 μM) electrochemical response in 0.1 M PBS at pH = 7.0 on the PPy NTs/GSPE was determined via linear sweep voltammetry (LSV). The corresponding data are shown in Figure 6. The hydroxylamine oxidation peak current (I_{pa}) was enhanced with an increasing scan rate from 10 to 500 mV/s and the peak potential shifted towards a more negative value, confirming the irreversibility of the oxidation reaction of hydroxylamine on the PPy NTs/GSPE. The peak current of the hydroxylamine oxidation was proportional to the scan rate square root ($v^{1/2}$) (Figure 6, inset), highlighting that the oxidation of hydroxylamine on the PPy NTs/GSPE was a typical diffusion-controlled electrode process, and the peak potential shifted towards a more negative value, confirming the irreversibility of the oxidation reaction of hydroxylamine on the PPy NTs/GSPE.

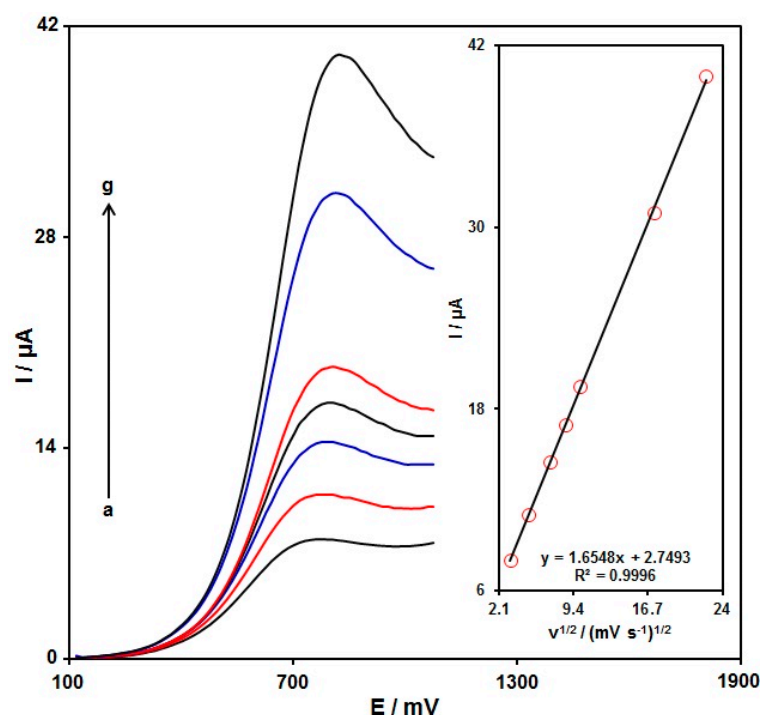


Figure 6. LSV recorded for the PPy NTs/GSPE in 0.1 M PBS at pH = 7 with 100.0 μM hydroxylamine at variable scan rates. Nos. a–g: 10, 25, 50, 75, 100, 300, and 500 mV/s, sequentially. Inset: variation of the anodic peak current versus $v^{1/2}$.

The rate-determining step was explored via the Tafel plot (Figure 7) according to the rising domain of the current–voltage curve at a scan rate of 10 mV/s. This section of the voltammogram (or the Tafel region) is influenced by electron transfer kinetics between the hydroxylamine and the PPy NTs/GSPE surface. The Tafel slope was 0.2555 and the charge transfer coefficient (α) was 0.77; thus, a two-electron transfer procedure can be discerned in the rate-determining step for the electro-oxidation of hydroxylamine.

3.4. Chronoamperometry

The hydroxylamine oxidation on the PPy NTs/GSPE was explored by chronoamperometry (Figure 8). Chronoamperometric determinations of the variable hydroxylamine contents on the PPy NTs/GSPE were performed at a working electrode potential of 840 mV. The obtained data were used to determine the diffusion coefficient (D) of the hydroxylamine. For the hydroxylamine as an electroactive material with a certain D value, Cottrell's equation was used to describe the current for the electrochemical reaction at a mass-transport-limited rate:

$$I = nFAD^{1/2}C_b\pi^{-1/2}t^{-1/2} \quad (1)$$

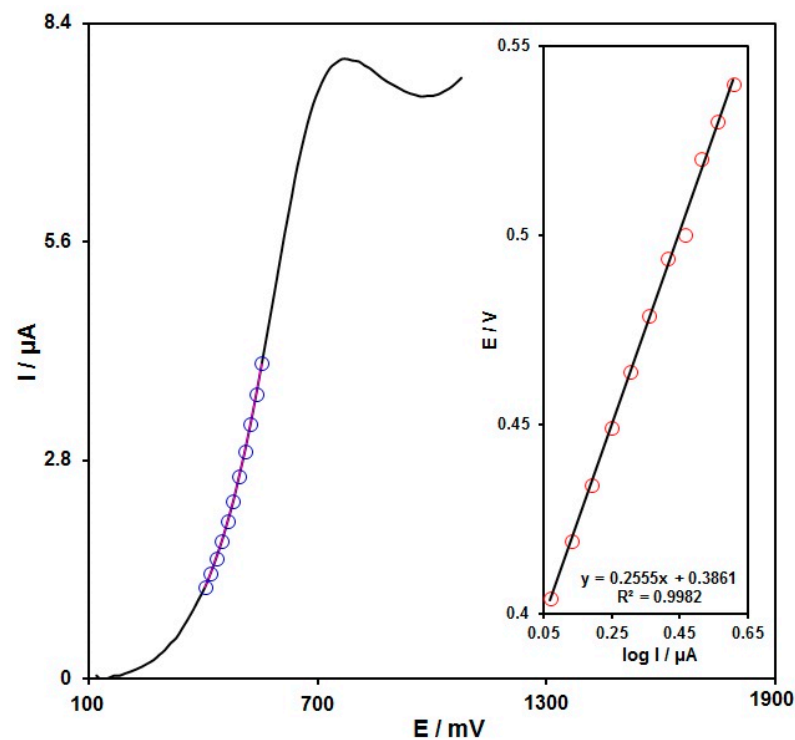


Figure 7. LSV recorded for the PPy NTs/GSPE at 10 mV/s in 0.1 M PBS at pH = 7 with 100.0 μM hydroxylamine. Points: data used in the Tafel plot. Inset: Tafel plot obtained from the LSV.

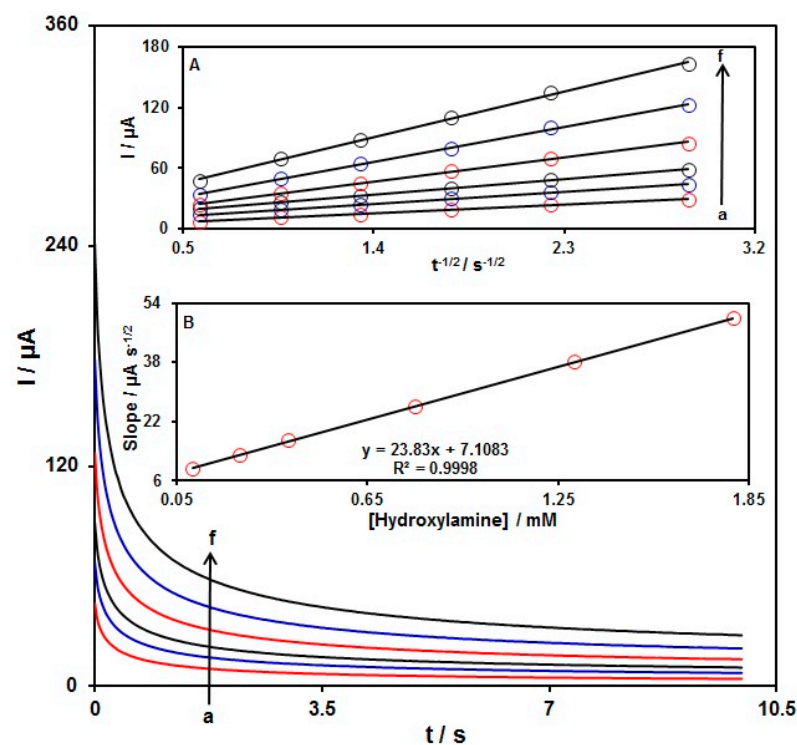


Figure 8. Chronoamperograms recorded for the PPy NTs/GSPE in 0.1 M PBS at pH = 7 with variable hydroxylamine contents. Nos. a–f: 0.1, 0.25, 0.4, 0.8, 1.3, and 1.8 mM of hydroxylamine. Insets: (A) Plots of I versus $t^{-1/2}$ derived from chronoamperograms a–f. (B) Corresponding slopes from the chronoamperogram curves vs. the hydroxylamine concentration.

In this equation, I stands for the current (A), n for the number of transferred electrons, F for the Faraday's constant, A for the electrode surface area (cm^2), t for time (s), C_b

for the bulk concentration (mol/cm^3), and D for the diffusion coefficient (cm^2/s). The experimental data of the I plot versus $t^{-1/2}$ are shown in Figure 8A, with the optimal fits for the various hydroxylamine contents. The achieved slopes of the straight lines in Figure 8A were plotted versus the hydroxylamine content (Figure 8B). The average D value of $4.8 \times 10^{-5} \text{ cm}^2/\text{s}$ was based on the obtained slope and on Cottrell's Equation (1).

3.5. Linear Dynamic Range and Limit of Detection

The standard curves were obtained by preparing multiple hydroxylamine solutions with various concentrations in 0.1 M PBS and measuring them on the PPy NTs/GSPE. Figure 9 illustrates a voltammogram of the DPVs at variable hydroxylamine contents (0.005, 0.07, 1.0, 5.0, 15.0, 30.0, 75.0, 100.0, 150.0, 200.0, 250.0, and 290.0 μM of hydroxylamine). According to our findings, there was an elevation in the peak currents with increasing hydroxylamine content. The standard curve of the DPV peak current for the hydroxylamine oxidation versus hydroxylamine concentration (Inset, Figure 9) demonstrates admirable linearity over a broad range of concentrations (0.005–290.0 μM) at $\text{pH} = 7$, with a correlation coefficient of 0.9998. In addition, the detection limit at 3σ equaled 0.001 μM . Table 1 lists the limit of detection and the linear range of the PPy NTs/GSPE compared with some modified electrodes used for hydroxylamine determination [56–61].

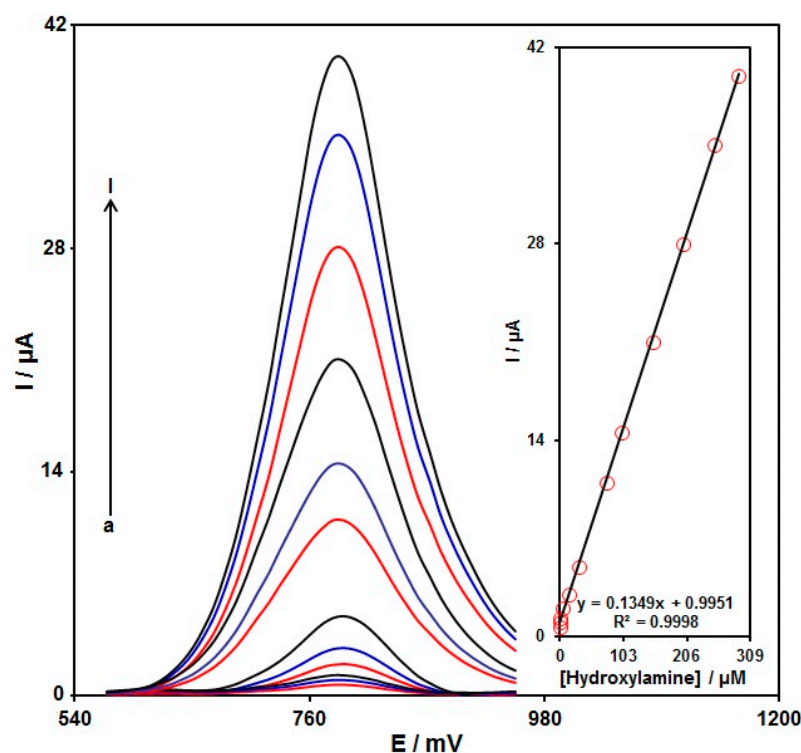


Figure 9. DPVs recorded for the PPy NTs/GSPE in 0.1 M (pH 7.0) with variable hydroxylamine concentrations. Nos. a–I: 0.005, 0.07, 1.0, 5.0, 15.0, 30.0, 75.0, 100.0, 150.0, 200.0, 250.0, and 290.0 μM of hydroxylamine. Inset: Plot of the electrocatalytic peak current as a function of the variable hydroxylamine concentrations (0.005–290.0 μM).

3.6. Stability, Repeatability, and Reproducibility

The long-term stability test of the PPy NTs/GSPE using DPV was performed at room temperature. The results exhibited that the peak current of 50.0 μM hydroxylamine on the PPy NTs/GSPE remained at 92.7% of its primary current after seven days, 91.9% after 14 days, and 88.7% after 21 days, indicating the superior long-term stability of the proposed sensor.

Table 1. Comparing the analytical performance of the PPy NTs/GSPE with other modified electrodes used for hydroxylamine determination.

Electrochemical Sensor	Method	Linear Range	Limit of Detection	Refs.
Graphene oxide/TiO ₂ /screen-printed electrode	Differential pulse voltammetry	0.1–300.0 µM	0.065 µM	[56]
Nickel(II)-morin complex modified multi-wall carbon nanotube paste electrode	Amperometry	2.5–400.0 µM	0.8 µM	[57]
Gold nanoparticle-polypyrrole nanowire/glassy carbon electrode	Differential pulse voltammetry	1.0–500.0 µM	0.21 µM	[58]
Gold nanoparticle-metal-metalloporphyrin frameworks/glassy carbon electrode	Differential pulse voltammetry	0.01–20.0 µM	0.004 µM	[59]
Cobalt(II) bis (benzoylacetone) ethylenediimino multi-wall carbon nanotube/carbon paste electrode	Square wave voltammetry	5.0–50.0 µM	12 µM	[60]
La ₂ O ₃ /Co ₃ O ₄ nanocomposite/onic liquid/carbon paste electrode	Differential pulse voltammetry	0.06–240.0 µM	3.0 nM	[61]
Polypyrrole nanotubes/graphite screen-printed electrode	Differential pulse voltammetry	0.005–290.0 µM	0.001 µM	This Work

The oxidation of hydroxylamine (50.0 µM) on the same PPy NTs/GSPE electrode was performed using ten repeated voltammetric measurements, the results of which confirmed the superior repeatability of the fabricated sensor, with a relative standard deviation (RSD) of 3.0%.

Similar conditions were provided for the measurement of the response currents of hydroxylamine (50.0 µM) on five PPy NTs/GSPEs, the results of which confirmed the excellent reproducibility of the fabricated sensor, with an RSD value of 3.7%.

3.7. Real Sample Analysis

The thus-fabricated sensor was examined for its applicability to the detection of hydroxylamine spiked in real specimens, including river (Halil, Jiroft, Iran) and well water (Graduate University of Advanced Technology, Kerman, Iran), by measuring via the standard addition method (Table 2). The spike recovery rate ranged from 96.7% to 104.3%, underlining the capacity of the modified electrodes for sensor applications in hydroxylamine determination in real specimens.

Table 2. Electrochemical determination of hydroxylamine in various water samples with the PPy NTs/GSPE. Concentrations are reported as µM ($n = 3$).

Sample	Spiked Concentration	Found Concentration	Recovery (%)	R.S.D. (%)
River water	0	-	-	-
	5.0	5.1	102.0	2.2
	7.5	7.3	104.3	3.0
Well water	0	-	-	-
	6.0	5.8	96.7	3.1
	7.0	7.1	101.4	2.0

4. Conclusions

We fabricated an ultra-sensitive electroanalytical sensor for hydroxylamine detection using the modification of a graphite screen-printed electrode based on polypyrrole nanotubes. The PPyNTs/GSPE was found to be a powerful platform for determining hydroxylamine in a range from 0.005 to 290.0 μM , voltammetrically. The limit of detection for hydroxylamine using the PPyNTs/GSPE was obtained as 0.001 μM . The recovery rate of 96.7% to 104.3% in real specimens verifies the appreciable potential of the newly developed sensor for sensing hydroxylamine in real specimens. As a result, it is evident that the PPyNTs/GSPE has an excellent electrochemical performance and potential for application as an electrochemical detection platform.

Author Contributions: Conceptualization, H.B. and A.D.B.; methodology, P.M.J. and H.B.; software, P.M.J.; validation, H.B. and A.D.B.; formal analysis, P.M.J., H.B. and A.D.B.; investigation, P.M.J. and H.B.; resources, P.M.J. and H.B.; data curation, A.D.B., P.M.J. and H.B.; writing—original draft preparation, P.M.J. and H.B.; writing—review and editing, A.D.B.; visualization, P.M.J.; supervision, H.B.; project administration, H.B. and A.D.B.; funding acquisition, P.M.J. and H.B. All authors have read and agreed to the published version of the manuscript.

Funding: This research received no external funding.

Institutional Review Board Statement: Not applicable.

Informed Consent Statement: Not applicable.

Data Availability Statement: The data presented in this study are available upon request from the corresponding authors.

Conflicts of Interest: The authors declare no conflict of interest.

References

1. Ensafi, A.A.; Heydari-Bafrooei, E.; Rezaei, B. Simultaneous detection of hydroxylamine and phenol using p-aminophenol-modified carbon nanotube paste electrode. *Chin. J. Catal.* **2013**, *34*, 1768–1775. [[CrossRef](#)]
2. Tajik, S.; Beitollahi, H.; Ahmadi, S.A.; Askari, M.B.; Di Bartolomeo, A. Screen-printed electrode surface modification with $\text{NiCo}_2\text{O}_4/\text{RGO}$ nanocomposite for hydroxylamine detection. *Nanomaterials* **2021**, *11*, 3208. [[CrossRef](#)]
3. Premalatha, S.; Chandrasekaran, M.; Bapu, G.R. Preparation of cobalt-RuO₂ nanocomposite modified electrode for highly sensitive and selective determination of hydroxylamine. *Sens. Actuators B Chem.* **2017**, *252*, 375–384. [[CrossRef](#)]
4. Zhang, C.; Wang, G.; Liu, M.; Feng, Y.; Zhang, Z.; Fang, B. A hydroxylamine electrochemical sensor based on electrodeposition of porous ZnO nanofilms onto carbon nanotubes films modified electrode. *Electrochim. Acta* **2010**, *55*, 2835–2840. [[CrossRef](#)]
5. Kannan, P.; John, S.A. Highly sensitive determination of hydroxylamine using fused gold nanoparticles immobilized on sol-gel film modified gold electrode. *Anal. Chim. Acta* **2010**, *663*, 158–164. [[CrossRef](#)] [[PubMed](#)]
6. Frear, D.S.; Burrell, R.C. Spectrophotometric method for determining hydroxylamine reductase activity in higher plants. *Anal. Chem.* **1955**, *27*, 1664–1665. [[CrossRef](#)]
7. Kumar, T.; Xavier, N.; Ramya, M. A High-Performance Liquid Chromatography Method for Determination of Genotoxic Impurity Hydroxylamine in Drug Substances. *J. Chromatogr. Sci.* **2019**, *57*, 63–70. [[CrossRef](#)]
8. Butler, J.H.; Gordon, L.I. An improved gas chromatographic method for the measurement of hydroxylamine in marine and fresh waters. *Mar. Chem.* **1986**, *19*, 229–243. [[CrossRef](#)]
9. Combeau, S.; Legeai, S.; Chatelut, M.; Vittori, O.; Devisme, F. Simultaneous determination of hydrogen peroxide, hydroxylamine and iodate in basic media by differential pulse polarography. *J. Nuclear Sci. Technol.* **2005**, *42*, 82–89. [[CrossRef](#)]
10. Sudha, V.; Annadurai, K.; Kumar, S.M.S.; Thangamuthu, R. CuCo_2O_4 nanobricks as electrode for enhanced electrochemical determination of hydroxylamine. *Ionics* **2019**, *25*, 5023–5034. [[CrossRef](#)]
11. Karimi-Maleh, H.; Beitollahi, H.; Kumar, P.S.; Tajik, S.; Jahani, P.M.; Karimi, F.; Zare, N. Recent advances in carbon nanomaterials-based electrochemical sensors for food azo dyes detection. *Food Chem. Toxicol.* **2022**, *164*, 112961. [[CrossRef](#)]
12. Ahmed, A.; Hayat, A.; John, P.; Nawaz, M.H.; Nasir, M. Coral-shaped tin oxide incorporated graphitic carbon nitride nanosheets as peroxidase mimic for sensitive colorimetric and fluorescence quenching based detection of hydrogen peroxide. *J. Nanostruct. Chem.* **2021**, *11*, 675–691.
13. Moghaddam, A.; Zamani, H.; Karimi-Maleh, H. A New Sensing Strategy for Determination of Tamoxifen Using $\text{Fe}_3\text{O}_4/\text{Graphene-Ionic Liquid Nanocomposite Amplified Paste Electrode}$. *Chem. Methodol.* **2021**, *5*, 373–380.
14. Dourandish, Z.; Tajik, S.; Beitollahi, H.; Jahani, P.M.; Nejad, F.G.; Sheikhshoae, I.; Di Bartolomeo, A. A Comprehensive Review of Metal–Organic Framework: Synthesis, Characterization, and Investigation of Their Application in Electrochemical Biosensors for Biomedical Analysis. *Sensors* **2022**, *22*, 2238. [[CrossRef](#)]

15. Montazarolmahdi, M.; Masrournia, M.; Nezhadali, A. A New Electrochemical Approach for the Determination of Phenylhydrazine in Water and Wastewater Samples using Amplified Carbon Paste Electrode. *Chem. Methodol.* **2020**, *4*, 732–742.
16. Karimi-Maleh, H.; Karimi, F.; Orooji, Y.; Mansouri, G.; Razmjou, A.; Aygun, A.; Sen, F. A new nickel-based co-crystal complex electrocatalyst amplified by NiO dope Pt nanostructure hybrid; a highly sensitive approach for determination of cysteamine in the presence of serotonin. *Sci. Rep.* **2020**, *10*, 11699. [[CrossRef](#)]
17. Shi, L.; Wu, T.; He, P.; Li, D.; Sun, C.; Li, J. Amperometric Sensor for Hydroxylamine Based on Hybrid Nickel-Cobalt Hexacyanoferrate Modified Electrode. *Electroanalysis* **2005**, *7*, 2190–2194. [[CrossRef](#)]
18. Fajardo, L.C.; Tamayo, A.I.B.; Guas, A.M.E. Characterization of graphite-epoxy composite electrodes for free electrochemical detection of adenine and guanine in DNA. *J. Electrochem. Sci. Eng.* **2021**, *11*, 247–261.
19. Mohanraj, J.; Durgalakshmi, D.; Rakkesh, R.A.; Balakumar, S.; Rajendran, S.; Karimi-Maleh, H. Facile synthesis of paper based graphene electrodes for point of care devices: A double stranded DNA (dsDNA) biosensor. *J. Colloid Interface Sci.* **2020**, *566*, 463–472. [[CrossRef](#)]
20. Tajik, S.; Beitollahi, H.; Shahsavari, S.; Nejad, F.G. Simultaneous and selective electrochemical sensing of methotrexate and folic acid in biological fluids and pharmaceutical samples using Fe₃O₄/PPy/Pd nanocomposite modified screen printed graphite electrode. *Chemosphere* **2022**, *291*, 132736. [[CrossRef](#)]
21. Ibáñez-Redín, G.; Wilson, D.; Gonçalves, D.; Oliveira, J. Low-cost screen-printed electrodes based on electrochemically reduced graphene oxide-carbon black nanocomposites for dopamine, epinephrine and paracetamol detection. *J. Colloid Interface Sci.* **2018**, *515*, 101–108. [[CrossRef](#)] [[PubMed](#)]
22. Shaikh, M.O.; Srikanth, B.; Zhu, P.Y.; Chuang, C.H. Impedimetric immunosensor utilizing polyaniline/gold nanocomposite-modified screen-printed electrodes for early detection of chronic kidney disease. *Sensors* **2019**, *19*, 3990. [[CrossRef](#)] [[PubMed](#)]
23. Tajik, S.; Dourandish, Z.; Nejad, F.G.; Aghaei Afshar, A.; Beitollahi, H. Voltammetric determination of isoniazid in the presence of acetaminophen utilizing MoS₂-nanosheet-modified screen-printed electrode. *Micromachines* **2022**, *13*, 369. [[CrossRef](#)] [[PubMed](#)]
24. Lee, S.; Lee, Y.J.; Kim, J.H.; Lee, G.J. Electrochemical Detection of H₂O₂ Released from Prostate Cancer Cells Using Pt Nanoparticle-Decorated rGO-CNT Nanocomposite-Modified Screen-Printed Carbon Electrodes. *Chemosensors* **2020**, *8*, 63. [[CrossRef](#)]
25. Tajik, S.; Askari, M.B.; Ahmadi, S.A.; Nejad, F.G.; Dourandish, Z.; Razavi, R.; Di Bartolomeo, A. Electrochemical sensor based on ZnFe₂O₄/RGO nanocomposite for ultrasensitive detection of hydrazine in real samples. *Nanomaterials* **2022**, *12*, 491. [[CrossRef](#)] [[PubMed](#)]
26. Geng, Y.; Ko, E.; Tran, V.K.; Chung, W.S.; Park, C.H.; Kim, M.K.; Seong, G.H. Electrochemical detection of hydroxylamine via Au-Pt alloy nanoparticle-modified single-walled carbon nanotube electrodes. *Anal. Sci.* **2017**, *33*, 993–998. [[CrossRef](#)]
27. Karimi-Maleh, H.; Sheikhsaie, M.; Sheikhsaie, I.; Ranjbar, M.; Alizadeh, J.; Maxakato, N.W.; Abbaspourrad, A. A novel electrochemical epinine sensor using amplified CuO nanoparticles and an-hexyl-3-methylimidazolium hexafluorophosphate electrode. *New J. Chem.* **2019**, *43*, 2362–2367. [[CrossRef](#)]
28. Pushpanjali, P.A.; Manjunatha, J.G.; Hareesha, N. An overview of recent developments of carbon-based sensors for the analysis of drug molecules Review. *J. Electrochem. Sci. Eng.* **2021**, *11*, 161–177.
29. Tajik, S.; Beitollahi, H.; Torkzadeh-Mahani, M. Electrochemical immunosensor for the detection of anti-thyroid peroxidase antibody by gold nanoparticles and ionic liquid-modified carbon paste electrode. *J. Nanostruct. Chem.* **2022**. [[CrossRef](#)]
30. Shahraki, S.; Masrournia, M.; Karimi-Maleh, H. Fabrication of Sulfapyridine Electrochemical Sensor Amplified with CuO/SWCNTs as High Performance Electroanalytical Tool in Real Sample Analysis. *Chem. Methodol.* **2020**, *4*, 720–731.
31. Li, J.; Xie, H.; Li, Y. Fabrication of gold nanoparticles/polypyrrole composite-modified electrode for sensitive hydroxylamine sensor design. *J. Solid State Electrochem.* **2012**, *16*, 795–802. [[CrossRef](#)]
32. Miraki, M.; Karimi-Maleh, H.; Taher, M.A.; Cheraghi, S.; Karimi, F.; Agarwal, S.; Gupta, V.K. Voltammetric amplified platform based on ionic liquid/NiO nanocomposite for determination of benserazide and levodopa. *J. Mol. Liq.* **2019**, *278*, 672–676. [[CrossRef](#)]
33. Moallem, Q.A.; Beitollahi, H. Electrochemical sensor for simultaneous detection of dopamine and uric acid based on a carbon paste electrode modified with nanostructured Cu-based metal-organic frameworks. *Microchem. J.* **2022**, *177*, 107261. [[CrossRef](#)]
34. Li, S.; Fan, J.; Li, S.; Ma, Y.; Wu, J.; Jin, H.; Guo, Z. In situ-grown Co₃O₄ nanorods on carbon cloth for efficient electrocatalytic oxidation of urea. *J. Nanostruct. Chem.* **2021**, *11*, 735–749.
35. Alavi-Tabari, S.A.; Khalilzadeh, M.A.; Karimi-Maleh, H. Simultaneous determination of doxorubicin and dasatinib as two breast anticancer drugs uses an amplified sensor with ionic liquid and ZnO nanoparticle. *J. Electroanal. Chem.* **2018**, *811*, 84–88. [[CrossRef](#)]
36. Haridas, V.; Yaakob, Z.; Sugunan, S.; Narayanan, B.N. Selective electrochemical determination of paracetamol using hematite/graphene nanocomposite modified electrode prepared in a green chemical route. *Mater. Chem. Phys.* **2021**, *263*, 124379. [[CrossRef](#)]
37. Baghernejad, B.; Rostami Harzevili, M. Nano-cerium Oxide/Aluminum Oxide: An Efficient and Useful Catalyst for the Synthesis of Tetrahydro[a]xanthenes-11-one Derivatives. *Chem. Methodol.* **2021**, *5*, 90–95.
38. Karimi-Maleh, H.; Karaman, C.; Karaman, O.; Karimi, F.; Vasseghian, Y.; Fu, L.; Mirabi, A. Nanochemistry approach for the fabrication of Fe and N co-decorated biomass-derived activated carbon frameworks: A promising oxygen reduction reaction electrocatalyst in neutral media. *J. Nanostruct. Chem.* **2022**, *12*, 429–439. [[CrossRef](#)]

39. Beitollahi, H.; Tajik, S.; Di Bartolomeo, A. Application of MnO₂ Nanorod–Ionic Liquid Modified Carbon Paste Electrode for the Voltammetric Determination of Sulfanilamide. *Micromachines* **2022**, *13*, 598. [[CrossRef](#)]
40. Zhang, X.; Yang, P.; Jiang, S.P. Horizontally growth of WS₂/WO₃ heterostructures on crystalline g-C₃N₄ nanosheets towards enhanced photo/electrochemical performance. *J. Nanostruct. Chem.* **2021**, *11*, 367–380. [[CrossRef](#)]
41. Karimi-Maleh, H.; Darabi, R.; Shabani-Nooshabadi, M.; Baghayeri, M.; Karimi, F.; Rouhi, J.; Karaman, C. Determination of D&C Red 33 and Patent Blue V Azo dyes using an impressive electrochemical sensor based on carbon paste electrode modified with ZIF-8/g-C₃N₄/Co and ionic liquid in mouthwash and toothpaste as real samples. *Food Chem. Toxicol.* **2022**, *162*, 112907.
42. Zhang, H.; Zheng, J. Sensitive detection of hydroxylamine at a simple baicalin carbon nanotubes modified electrode. *Talanta* **2012**, *93*, 67–71. [[CrossRef](#)]
43. Nejad, F.G.; Sheikhshoae, I.; Beitollahi, H. Simultaneous detection of carmoisine and tartrazine in food samples using GO-Fe₃O₄-PAMAM and ionic liquid based electrochemical sensor. *Food Chem. Toxicol.* **2022**, *162*, 112864. [[CrossRef](#)]
44. Eren, T.; Atar, N.; Yola, M.L.; Karimi-Maleh, H. A sensitive molecularly imprinted polymer based quartz crystal microbalance nanosensor for selective determination of lovastatin in red yeast rice. *Food Chem.* **2015**, *185*, 430–436. [[CrossRef](#)]
45. Payehghadr, M.; Taherkhani, Y.; Maleki, A.; Nourifard, F. Selective and sensitive voltammetric sensor for methocarbamol determination by molecularly imprinted polymer modified carbon paste electrode. *Eurasian Chem. Commun.* **2020**, *2*, 982–990.
46. Lin, M.; Hu, X.; Ma, Z.; Chen, L. Functionalized polypyrrole nanotube arrays as electrochemical biosensor for the determination of copper ions. *Anal. Chim. Acta* **2012**, *746*, 63–69. [[CrossRef](#)] [[PubMed](#)]
47. Velhal, N.; Kulkarni, G.; Patil, N.D.; Puri, V. Structural, electrical and microwave properties of conducting polypyrrole thin films: Effect of oxidant. *Mater. Res. Express* **2018**, *5*, 106407. [[CrossRef](#)]
48. Lin, M. A dopamine electrochemical sensor based on gold nanoparticles/over-oxidized polypyrrole nanotube composite arrays. *RSC Adv.* **2015**, *5*, 9848–9851. [[CrossRef](#)]
49. Ding, S.; Lyu, Z.; Li, S.; Ruan, X.; Fei, M.; Zhou, Y.; Lin, Y. Molecularly imprinted polypyrrole nanotubes based electrochemical sensor for glyphosate detection. *Biosens. Bioelectron.* **2021**, *191*, 113434. [[CrossRef](#)] [[PubMed](#)]
50. Kannan, A.; Radhakrishnan, S. Fabrication of an electrochemical sensor based on gold nanoparticles functionalized polypyrrole nanotubes for the highly sensitive detection of l-dopa. *Mater. Today Commun.* **2020**, *25*, 101330. [[CrossRef](#)]
51. Yashas, S.R.; Sandeep, S.; Shivakumar, B.P.; Swamy, N.K. A matrix of perovskite micro-seeds and polypyrrole nanotubes tethered laccase/graphite biosensor for sensitive quantification of 2,4-dichlorophenol in wastewater. *Anal. Methods* **2019**, *11*, 4511–4519. [[CrossRef](#)]
52. Ye, S.; Feng, J. Self-assembled three-dimensional hierarchical graphene/polypyrrole nanotube hybrid aerogel and its application for supercapacitors. *ACS Appl. Mater. Interfaces* **2014**, *6*, 9671–9679. [[CrossRef](#)]
53. Liu, J.; An, J.; Ma, Y.; Li, M.; Ma, R. Synthesis of a graphene-polypyrrole nanotube composite and its application in supercapacitor electrode. *J. Electrochem. Soc.* **2012**, *159*, A828. [[CrossRef](#)]
54. Zhang, D.; Zhang, X.; Chen, Y.; Yu, P.; Wang, C.; Ma, Y. Enhanced capacitance and rate capability of graphene/polypyrrole composite as electrode material for supercapacitors. *J. Power Sources* **2011**, *196*, 5990–5996. [[CrossRef](#)]
55. Yussuf, A.; Al-Saleh, M.; Al-Enezi, S.; Abraham, G. Synthesis and characterization of conductive polypyrrole: The influence of the oxidants and monomer on the electrical, thermal, and morphological properties. *Int. J. Polym. Sci.* **2018**, *2018*, 4191747. [[CrossRef](#)]
56. Malakootian, M.; Gholami, Z.; Mahmoudi-Moghaddam, H. Electrochemical determination of hydroxylamine in water samples using modified screen-printed electrode with TiO₂/GO. *Int. J. Environ. Anal. Chem.* **2021**, *101*, 35–47. [[CrossRef](#)]
57. Zheng, L.; Song, J.F. Electrocatalytic oxidation of hydroxylamine at Ni (II)-morin complex modified carbon nanotube paste electrode. *J. Appl. Electrochem.* **2011**, *41*, 63–70. [[CrossRef](#)]
58. Li, J.; Lin, X. Electrocatalytic oxidation of hydrazine and hydroxylamine at gold nanoparticle—polypyrrole nanowire modified glassy carbon electrode. *Sens. Actuators B Chem.* **2007**, *126*, 527–535. [[CrossRef](#)]
59. Wang, Y.; Wang, L.; Chen, H.; Hu, X.; Ma, S. Fabrication of highly sensitive and stable hydroxylamine electrochemical sensor based on gold nanoparticles and metal–metalloporphyrin framework modified electrode. *ACS Appl. Mater. Interfaces* **2016**, *8*, 18173–18181. [[CrossRef](#)]
60. Benvidi, A.; Kakoolaki, P.; Gorji, A.R.; Mazloum-Ardakani, M.; Zare, H.R.; Vafazadeh, R. Application of Co (II) complex multi-wall carbon nanotube modified carbon paste electrodes for electrocatalytic determination of hydroxylamine. *Anal. Methods* **2013**, *5*, 6649–6655. [[CrossRef](#)]
61. Nazari, M.; Asadollahzadeh, H.; Shahidi, M.; Rastakhiz, N.; Mohammadi, S.Z. Sensitive determination of hydroxylamine by using modified electrode by La₂O₃–Co₃O₄ nanocomposite and ionic liquid. *Mater. Chem. Phys.* **2022**, *286*, 126209. [[CrossRef](#)]